AGU PUBLICATIONS

Journal of Advances in Modeling Earth Systems

RESEARCH ARTICLE
10.1002/2016MS000815

Key Points:
- A new computational framework (FIVE) for better representation of low and high clouds in large-scale models is proposed
- FIVE embeds process calculations with locally high vertical resolution grid for PBL and cirrus regions in the host model
- FIVE produces comparable results to a reference high-resolution simulation but at reduced computational cost

Correspondence to:
T. Yamaguchi,
tak.yamaguchi@noaa.gov

Citation:
Yamaguchi, T., G. Feingold, and V. E. Larson (2017), Framework for improvement by vertical enhancement: A simple approach to improve representation of low and high-level clouds in large-scale models, *J. Adv. Model. Earth Syst.*, *9*, 627–646, doi:10.1002/2016MS000815.

Received 21 SEP 2016
Accepted 27 FEB 2017
Accepted article online 2 MAR 2017
Published online 23 MAR 2017

Framework for improvement by vertical enhancement: A simple approach to improve representation of low and high-level clouds in large-scale models

Takanobu Yamaguchi[1,2], Graham Feingold[2], and Vincent E. Larson[3]

[1]Cooperative Institute for Research in Environmental Sciences, University of Colorado, Boulder, Colorado, USA, [2]NOAA Earth System Research Laboratory, Boulder, Colorado, USA, [3]Department of Mathematical Sciences, University of Wisconsin-Milwaukee, Milwaukee, Wisconsin, USA

Abstract Low and high clouds of shallow extent, especially stratocumulus and even more so for high-level cirrus clouds that reside where vertical resolution is particularly coarse, are poorly represented in large-scale models such as global climate models and weather forecasting models. This adversely affects, among others, estimation of cloud feedbacks for climate prediction and weather forecasts. Here we address vertical resolution as a reason for the failure of these models to adequately represent shallow clouds. We introduce a new methodology, the Framework for Improvement by Vertical Enhancement (FIVE). FIVE computes selected processes on a one-dimensional vertical grid with local high resolution in the boundary layer and near the tropopause. In addition to the host model, variables on the locally high-resolution grid are predicted in parallel so that high-resolution information is retained. By exchanging tendencies with one another, the host model and high-resolution field are always synchronized. The methodology is demonstrated for drizzling stratocumulus capped by a sharp inversion. First, FIVE is applied to a single-column model to identify the cause of biases associated with computing an assigned process at low resolution. Second, a two-dimensional regional model coupled with FIVE is shown to produce results comparable to those performed with high vertical resolution. FIVE is thus expected to represent low clouds more realistically and hence reduce the low-cloud bias in large-scale models. Finally, we propose a number of methods that will be developed and tested to further optimize FIVE.

1. Introduction

In atmospheric science, the "cloud parameterization problem" is endemic in applications as widespread as the cloud-climate feedback, the prediction of precipitation, and solar energy management. Poor representation of clouds compromises our ability to determine the magnitude and even the sign of the cloud feedback in climate simulations and to accurately predict precipitation in weather forecast models. Clouds interact with large-scale dynamical and hydrological processes. The interactions are two-way; thus, cloud parameterization and large-scale circulation are intricately linked [e.g., *Arakawa*, 1975, 2004]. *Arakawa* [2004] emphasizes the need for a "unified cloud parameterization" or even "unified model physics," designed to represent both cumuliform and stratiform clouds with one physical framework. The problem is particularly pertinent to low-level clouds in the planetary boundary layer (PBL), given their strong relationship with climate sensitivity [*Bony and Dufresne*, 2005; *Nam et al.*, 2012; *Sherwood et al.*, 2014].

In recent years, the development of PBL parameterizations has been geared toward unification. One particular example is the application of higher-order closure (HOC) models with assumed probability density functions (PDFs) [*Lappen and Randall*, 2001a, 2001b, 2001c; *Larson et al.*, 2001, 2002; *Golaz et al.*, 2002a, 2002b; *Larson and Golaz*, 2005; *Cheng et al.*, 2004; *Cheng and Xu*, 2006, 2009; *Bogenschutz and Krueger*, 2013; *Griffin and Larson*, 2016]. The HOC-PDF model predicts turbulence statistics, i.e., higher-order moments, of velocity as well as thermodynamic scalars, and closes the system of equations by assuming a particular PDF, e.g., double delta or double Gaussian. Condensation amount and cloud fraction are also obtained from the PDFs.

These HOC models have been applied to the single-column model (SCM) mode of global climate models (GCMs) [*Cheng and Xu*, 2009, 2015; *Guo et al.*, 2010, 2011; *Bogenschutz et al.*, 2012], cloud system resolving models (CSRMs) [*Cheng and Xu*, 2006; *Larson et al.*, 2012; *Bogenschutz and Krueger*, 2013], and GCMs

[*Bogenschutz et al*., 2013; *Guo et al*., 2014, 2015; *Cheng and Xu*, 2015; *Thayer-Calder et al*., 2015]. *Cheng and Xu* [2013a, 2013b], *Xu and Cheng* [2013a, 2013b], and *Wang et al*. [2015] used their HOC model in a two-dimensional (2-D) CSRM within the Multiscale Modeling Framework (MMF) [*Grabowski*, 2001; *Khairoutdinov and Randall*, 2001; *Randall et al*., 2003; *Khairoutdinov et al*., 2005]. MMF embeds a CSRM into each GCM column and computes feedbacks to the large-scale field with statistics obtained by running a CSRM inside each GCM column.

HOC-PDF models improve the representation of low clouds in GCMs compared with their predecessors; e.g., a more gradual transition from the stratocumulus regime to the trade cumulus regime, although there is still large room for improvement in, e.g., geographical distribution of low-cloud cover, low-cloud water amount, and thus the shortwave radiative effect associated with low clouds. GCM results are further improved when these HOC models are used to represent PBL turbulence at high resolution; for vertical resolution this improvement is also apparent in SCM, CSRM, and MMF.

These results imply that poor vertical resolution in the HOC model may be a significant cause of low-cloud bias, even though the HOC model is theoretically and physically consistent. If so, this would be germane to any PBL parameterization that exhibits sensitivity to vertical resolution when used in large-scale models such as CSRM, GCM, MMF, as well as regional weather forecast models. (Considering the use of CSRM as a global model [e.g., *Miura et al*., 2007], we include CSRM in the large-scale model category.)

The above hypothesis regarding degraded performance of a parameterization due to poor vertical resolution is also applicable to high clouds, i.e., cirrus clouds. GCMs have difficulty in simulating the appropriate distribution of cirrus clouds [*Waliser et al*., 2009; *Li et al*., 2012]. While the observed thickness of a cirrus cloud layer is typically 1–2 km, the vertical resolution in these GCMs near the tropopause where cirrus clouds reside is about 1 km. Recently, *Seiki et al*. [2015] demonstrated with a global CSRM that increasing the vertical resolution around the tropopause improves agreement with observed radiative properties in the subtropics.

Although not discussed explicitly, mixed phase boundary layer clouds in the high latitudes (Arctic and Southern Ocean) are notoriously difficult to represent in large-scale models [*Trenberth and Fasullo*, 2010]. The reasons for this are partially microphysical (e.g., poor understanding of ice nucleating particles and mixed phase microphysics) but to a large extent because of poor vertical resolution. While mixed phase boundary layer clouds are not the focus of this study, our expectation is that they will also benefit significantly from higher vertical resolution.

Development of cloud parameterizations to improve biases in large-scale models is time-consuming. While new parameterization development is undoubtedly important, a method that maximizes the full potential of *existing* cloud parameterizations is desired to advance our climate predictions with moderate increase in computational cost. Focusing on the sensitivity to vertical resolution for HOC-based turbulence parameterizations, we develop and present such a method in this study and refer to it as the Framework for Improvement by Vertical Enhancement (FIVE).

Our focus for FIVE is an assessment of whether each parameterized process has sufficient vertical resolution to produce acceptable results, and at reasonable cost. If so, the overall model performance will improve when computing each process at the higher vertical resolution. The idea has been used for the temporal scale by applying sub-time stepping for specific processes to achieve desired accuracy and stability. For example, in large eddy simulations (LESs) as well as CSRMs, the interactive radiation calculation is often performed with a longer time step, which is specified after consideration of the balance between bias and cost.

FIVE operates as follows. Separate from the host model, FIVE creates an additional vertical grid in each grid column that has locally high resolution for PBL and cirrus regions. In parallel to the host model, FIVE allocates prognostic variables on the locally high-resolution grid and predicts them by computing selected one-dimensional (1-D) processes on the locally high-resolution grid as well as applying interpolated tendencies from the host model for other processes. The embedded process calculation as well as prediction on the locally high-resolution grid is called Vertically Enhanced Physics (VEP). FIVE is designed so that it does not interfere with the order of the computation of processes in the host model. For instance, if the host model sequence of processes is A, B, C, D, and E, and processes B, C, and E are selected for calculation within VEP, then the order will be: process A (host model) → process B (VEP) → process C (VEP) → process D

(host model) → process E (VEP). In this way there is no double-counting of processes between the host model and VEP. The averaged tendency computed in VEP is applied to the host model for prediction. Whenever the sequence of processes requires moving between host model and VEP, the host model and VEP are synchronized by exchanging tendencies with one another to prevent any drift in the host model state. For the high-resolution region of the VEP grid, the resolvable scale is smaller than in the host model. By averaging the VEP tendency and interpolating the host model tendency, FIVE maintains the scale separation between the host model and VEP.

FIVE shares similarities to existing numerical methods such as MMF, multigrid methods [e.g., *Brandt*, 1977; *Fulton et al*., 1986], and the grid nesting method [e.g., *Clark and Farley*, 1984]. VEP is embedded in all columns of the host model, which is similar to embedding a CSRM in MMF. Since processes in VEP are only computed in the vertical direction, there is no communication between VEP columns, which is similar to MMF without the quasi-3-D approach [*Randall et al*., 2003]. FIVE uses the same parameterizations and numerical schemes used in the host model, which is similar to the grid nesting method. FIVE's synchronization strategy follows MMF but in the vertical direction. For FIVE's synchronization, tendencies are exchanged back and forth between host model and VEP through interpolation and averaging, which is similar to "prolongation" (interpolation to the finer grid) and "restriction" (averaging back to the coarser grid) in multigrid methods. *Brandt* [1977] states "Another point of view is to regard finer grids as the correction grids, improving accuracy on coarser grids by correcting their forcing terms." This is exactly the aim of FIVE. For the prolongation of FIVE, we have developed a monotonic interpolation scheme that conserves tendencies, i.e., averaging the interpolant over VEP levels within a host model layer gives the tendency at the corresponding level of the host model.

A detailed description of FIVE and the performance of the prototype FIVE are given in sections 2 and 3, respectively. We will show that the prototype FIVE produces superior results for SCM and 2-D regional model simulations compared with those performed with low vertical resolution in the host model. The prototype FIVE also produces results comparable to those performed with the high vertical resolution model, while saving computational cost. In section 4, a number of ideas for further development of FIVE are discussed, and summary and conclusions are given in section 5.

2. Framework for Improvement by Vertical Enhancement (FIVE)

2.1. Method

The locally high-resolution vertical VEP grid has to be constructed so that it matches the host model levels when the resolution between these two is the same. This ensures that FIVE produces the same results compared with a standalone host model simulation when the two models share common levels. For the model used in this study, which employs the Arakawa C-grid, in order to be able to aggregate fine-grid tendencies back to the coarse grid, each interface level of the host model grid needs to match the interface level of the VEP grid

$$\ldots < \begin{bmatrix} \hat{Z}_K \\ \hat{z}_{k-n} \end{bmatrix} < z_{k-n} < \ldots < \hat{z}_k < \begin{bmatrix} Z_K \\ z_k \end{bmatrix} < \hat{z}_{k+1} < \ldots < z_{k+n} < \begin{bmatrix} \hat{Z}_{K+1} \\ \hat{z}_{k+n+1} \end{bmatrix} < \ldots , \tag{1}$$

where Z_K is the K-th level of the host model (for thermodynamic variables and horizontal velocity), and $\hat{Z}$ denotes the interface level (level for vertical velocity); z_k is the k-th level of VEP and $\hat{z}$ denotes the interface level; the heights inside the brackets are the same, i.e., $Z_K = z_k$; $2n$ is the number of additional levels within a host model layer between $\hat{Z}_K$ and $\hat{Z}_{K+1}$. Throughout the paper, upper (lower) case letters are used to denote host model (VEP). Also, note that K and k indices will generally have different values. A total of $2n+1$ VEP levels are placed within a host model layer, e.g., between $\hat{Z}_K$ and $\hat{Z}_{K+1}$. The value of n can be varied with K; for instance, $n \geq 0$ within the region of vertical enhancement (i.e., high resolution), and $n = 0$ above it. The fine resolution is extended to some height above the PBL to capture the sharp inversion associated with stratocumulus clouds. For cirrus clouds, local high resolution is used near the upper troposphere.

Here we consider systems with time-independent density, e.g., Boussinesq or anelastic systems. A short discussion of compressible systems is given in Appendix A. In order to accurately capture the initial vertical gradient in VEP, FIVE first initializes the VEP profiles, and then the host model profiles are computed as a

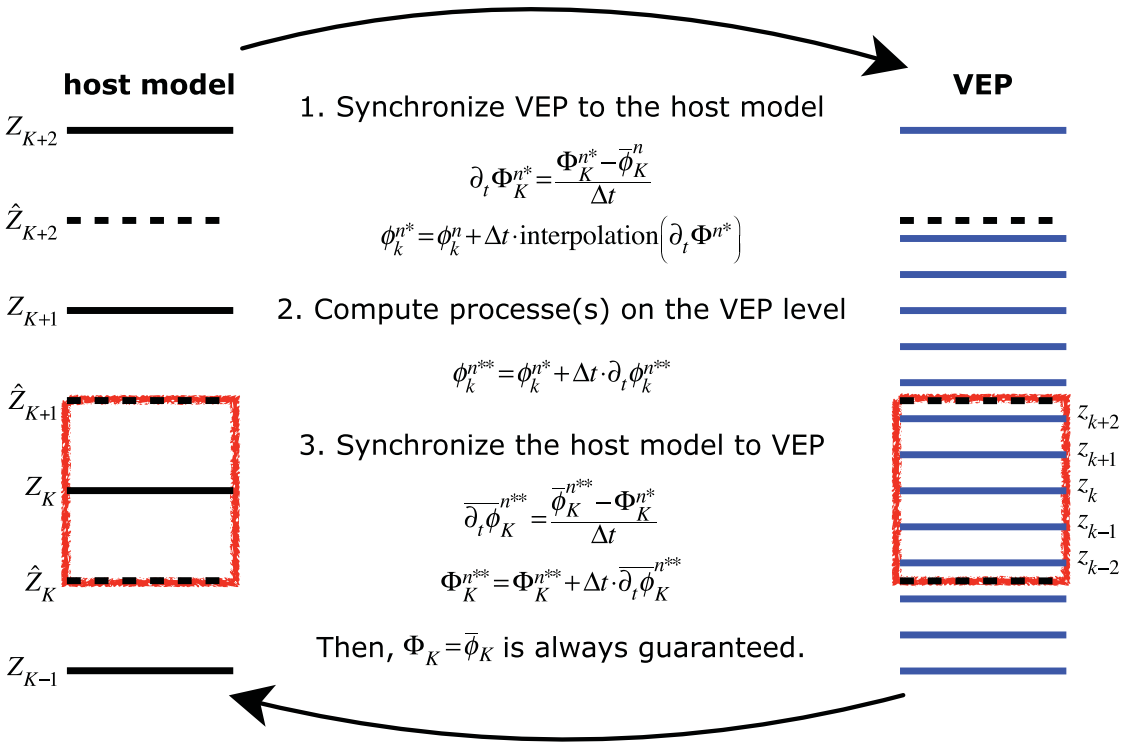

Figure 1. Schematic of FIVE. For this example, VEP has 5 times higher resolution than the host model in the vertically enhanced region below $\hat{Z}_{K+2}$. Upper case symbols are used to denote the host model while lower case symbols are used for VEP. The black dashed line is used for the host model interface levels. z_k is located at Z_K. A host model layer at Z_K is shown as a red box (i.e., between $\hat{Z}_K$ and $\hat{Z}_{K+1}$). All notations are defined in the text.

mass-weighted vertical average over a host model layer, which will be called the host model layer mean, written as

$$\Phi_K = \bar{\phi}_K = \frac{\sum_{i=k-n}^{k+n} (\phi \rho \delta z)_i}{\sum_{i=k-n}^{k+n} (\rho \delta z)_i} = \frac{1}{R_K \Delta Z_K} \sum_{i=k-n}^{k+n} (\phi \rho \delta z)_i \,, \tag{2}$$

where Φ is a prognostic variable defined on the host model level; ϕ is a prognostic variable defined on the VEP level; the overbar denotes a host model layer mean; ρ is the air density for VEP; δz is the vertical grid spacing for the VEP level z (i.e., $\delta z_k = \hat{z}_{k+1} - \hat{z}_k$); R is the air density for the host model; ΔZ is the vertical grid spacing for the host model level Z (i.e., $\Delta Z_K = \hat{Z}_{K+1} - \hat{Z}_K$); and

$$R_K = \bar{\rho}_K = \frac{1}{\Delta Z_K} \sum_{i=k-n}^{k+n} (\rho \delta z)_i \,. \tag{3}$$

Figure 1 illustrates the methodology employed by FIVE. Prior to the VEP calculation, FIVE synchronizes VEP to the host model just as in MMF. Here we consider a time splitting scheme so that prognostic thermodynamic variables are updated sequentially with every process. We also ensure that $\bar{\phi}_K = \Phi_K$ is satisfied at the beginning of the time step. Assume that processes have been computed only in the host model at this point. In this case only Φ_K has been partially updated. The total tendency on the host model, which has been added to Φ_K, is calculated as

$$\partial_t \Phi_K^{n*} = \frac{\Phi_K^{n*} - \bar{\phi}_K^n}{\Delta t} \,, \tag{4}$$

where $\partial_t \equiv \frac{\partial}{\partial t}$; the superscript n denotes the time step index for the host model; the superscript, $n*$, denotes a partially incremented time step between n and $n+1$; and Δt is the host model time step. Since $\partial_t \Phi_K^{n*}$ is

defined on the host model level, it has to be interpolated to the VEP level, and an interpolation scheme must satisfy $\overline{\partial_t \phi}_K^{n*} = \partial_t \Phi_K^{n*}$. Such an interpolation method is developed and described in Appendix B. With the interpolated tendency, ϕ is updated as

$$\begin{aligned} \phi_k^{n*} &= \phi_k^n + \Delta t \cdot \text{interpolation}(\partial_t \Phi^{n*}) \\ &= \phi_k^n + \Delta t \cdot \partial_t \phi_k^{n*}, \end{aligned} \tag{5}$$

where the interpolation scheme requires the entire profile of $\partial_t \Phi^{n*}$ (Appendix B). The synchronization of VEP to the host model is completed and $\bar{\phi}_K^{n*} = \Phi_K^{n*}$ is satisfied.

In VEP, ϕ_k^{n*} is updated to ϕ_k^{n**} by applying a tendency computed on the VEP level,

$$\phi_k^{n**} = \phi_k^{n*} + \Delta t \cdot \partial_t \phi_k^{n**}. \tag{6}$$

The calculation may require sub-time stepping when a process requires a smaller time step than Δt in which case this update is repeated for that process. When subsequent processes are assigned to be computed in VEP, ϕ is progressively updated by (6).

Before returning to the host model, FIVE synchronizes the host model to VEP. The net VEP tendency on the host model level is given with the host model layer mean as

$$\overline{\partial_t \phi}_K^{n**} = \frac{\bar{\phi}_K^{n**} - \Phi_K^{n*}}{\Delta t}, \tag{7}$$

after which the host model is updated by

$$\Phi_K^{n**} = \Phi_K^{n*} + \Delta t \cdot \overline{\partial_t \phi}_K^{n**}. \tag{8}$$

One sees that $\bar{\phi}_K^{n**} = \Phi_K^{n**}$ is guaranteed even when VEP computes no process, in which case VEP is updated only with the host model tendency.

FIVE's interpolation method is applied to the tendency computed on the host model level, but not to construct the profiles of each prognostic variable, so that important information such as profiles around the inversion is retained and available whenever necessary. Although one could argue that a profile can be reconstructed [e.g., *Grenier and Bretherton*, 2001], our experience has shown that reconstructing the inversion profile with interpolation techniques is problematic because the inversion height changes with time and it is difficult to estimate the inversion height, scalar values, and their vertical gradients at any given time. A conclusion of our current work is that predicting a scalar on a high-resolution level with the interpolated *tendency* from a low-resolution level appears to represent the evolution of the inversion better than diagnosing/reconstructing the scalar itself by interpolation.

2.2. Local Vertical Mesh Refinement

Since FIVE maintains memory of both host model and VEP states, one way to minimize the error associated with interpolating the host model tendency is to use preexisting VEP levels for a particularly important region for that process, e.g., radiation at stratocumulus cloud top. This can be done by computing a process with temporarily constructed local high-resolution profiles such that a limited range of the VEP profile is embedded into the host model profile (Figure 2b). The higher vertical resolution is added ad hoc, for example for calculating radiation around a sharp gradient associated with stratocumulus cloud top. A process is calculated at high vertical resolution (as in VEP) over a limited altitude range, where the process is deemed to be needed most (e.g., stratocumulus cloud top). After the calculations, the tendency is applied to both host model and VEP. The computed process tendency over the local high resolution is layer-averaged and then applied to the host model. For VEP, the tendency profile outside the local high resolution is interpolated. We refer to this method as "local vertical mesh refinement." As shown in Figure 2a, the method starts with synchronization between the host model and VEP, construction of local high-resolution profiles, computing the process with the local high-resolution profiles, and finally application of the computed tendency to both host model and VEP. The goal of the local vertical mesh refinement is to maximize the accuracy of the computed process while minimizing the associated cost. It will be shown later that this local vertical mesh refinement method maintains accuracy of radiative heating as if it were computed over the full altitude range of the high-resolution profile.

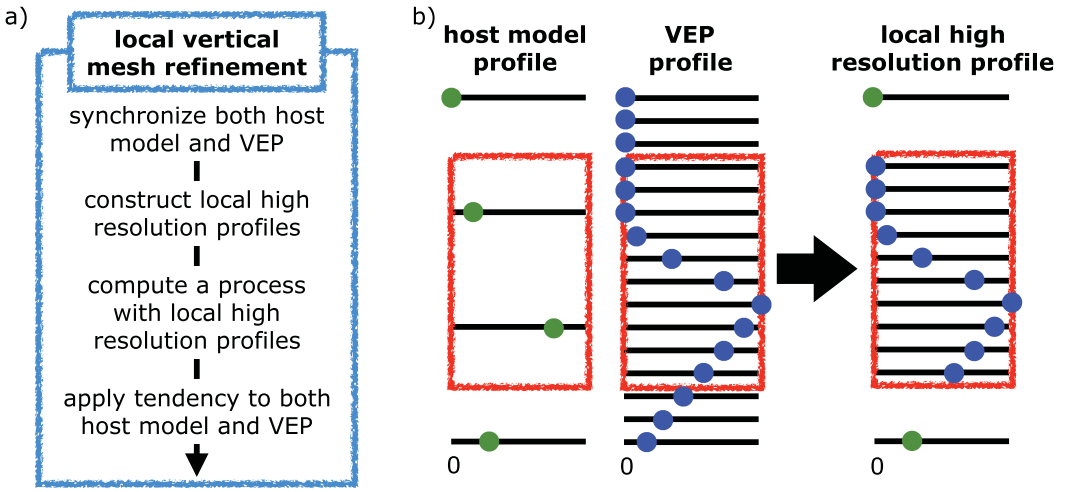

Figure 2. Schematic of a local vertical mesh refinement for FIVE; (a) algorithmic flowchart for the method and (b) example for constructing local high-resolution profile. In this example, the green and blue filled circles represent cloud water condensate on levels of the host model and VEP, respectively, and the high-resolution profile around cloud top is inserted into the low-resolution profile to generate a local high-resolution profile.

3. Testing FIVE

3.1. Prototype FIVE

A prototype version of FIVE has been implemented into the System for Atmospheric Modeling (SAM) [*Khairoutdinov and Randall*, 2003] coupled with the HOC turbulence parameterization scheme known as Cloud Layers Unified By-Binormals (CLUBB) [*Larson and Golaz*, 2005]. SAM is a nonhydrostatic model formulated as an anelastic system with Arakawa C-grid spatial discretization. A time splitting scheme is used to predict thermodynamic variables, while velocity is predicted with the third-order Adams-Bashforth scheme [*Durran*, 1991] in a process-splitting manner, such that tendencies are calculated with the variables at the same time step and then added for prognosis. The third-order Adams-Bashforth scheme is written as

$$\mathbf{U}^{n+1}=\mathbf{U}^{n}+\Delta t\left(\alpha_n\partial_t\mathbf{U}^{n}+\alpha_{n-1}\partial_t\mathbf{U}^{n-1}+\alpha_{n-2}\partial_t\mathbf{U}^{n-2}\right), \tag{9}$$

where $\mathbf{U}$ is velocity, and α_n, α_{n-1}, and α_{n-2} are coefficients. CLUBB is a third-order closure model with a double-Gaussian (binormal PDF) representation. It predicts all first moments except vertical velocity, which is an input variable to CLUBB, all second moments, and the third moment of vertical velocity, and closes other third and higher moments with a double Gaussian.

The prototype FIVE has an option to compute turbulence, microphysics, radiation, and/or advection due to externally prescribed vertical velocity (subsidence) in either the host model (i.e., SAM) or VEP. We use this setup to assess the bias caused by computing selected physical processes on the coarse resolution host model vertical grid. Prognostic variables in VEP are the thermodynamic variables and the horizontal velocity component. Advection due to resolved-scale vertical velocity, which will develop in the 2-D simulations discussed below, is processed in the host model. For the horizontal velocity component ($\mathbf{U}_H$ for the host model and $\mathbf{u}_H$ for VEP, where the subscript H denotes horizontal components), subsidence is always computed in the host model, so that the only process that can be computed in VEP is the turbulent tendency (by CLUBB). Because SAM's velocity is predicted by the third-order Adams-Bashforth scheme, which uses the total tendency at the current and past two time steps, $\mathbf{u}_H$ is also predicted with the same scheme, in order to apply the high-resolution CLUBB tendency on the VEP level directly to $\mathbf{u}_H$ as well as meet $\mathbf{U}_H=\overline{\mathbf{u}}_H$. When CLUBB is processed in VEP, the total tendencies of $\mathbf{U}$ and $\mathbf{u}_H$ are computed by

$$\partial_t\mathbf{U}^{n}=\left(\overline{\partial_t\mathbf{u}_H}\right)^{n}_{\mathrm{CLUBB}}+\partial_t\mathbf{U}^{n}_{\mathrm{other}}, \tag{10a}$$

$$\partial_t\mathbf{u}_H^{n}=\left(\partial_t\mathbf{u}_H^{n}\right)_{\mathrm{CLUBB}}+\mathrm{interpolation}\left[\left(\partial_t\mathbf{U}_H^{n}\right)_{\mathrm{other}}\right]. \tag{10b}$$

Note that vertical velocity is a prognostic variable in SAM while it is an input variable for CLUBB. Thus, vertical velocity is a diagnostic variable in VEP, and linear interpolation is used to construct it on the VEP levels.

3.2. Case Study Description

The nocturnal drizzling stratocumulus case of DYCOMS-II RF02 [*Ackerman et al*., 2009] is used to test FIVE. The microphysics scheme of *Khairoutdinov and Kogan* [2000] with a prescribed droplet number concentration of 55 cm^{-3} is used in conjunction with the cloud water sedimentation scheme of *Ackerman et al*. [2009]. Radiation is computed with the simple radiation parameterization of *Stevens et al*. [2005], and as an option, the local vertical mesh refinement is implemented for radiation near the cloud top (Figure 2). Subsidence is prescribed in the host model as a function of height with large-scale horizontal wind divergence, 3.75×10^{-6} s^{-1}, and is linearly interpolated to the VEP level.

All simulations presented in this study use a 16 km horizontal grid spacing, a 20 s time step, and a 3 km model top. Compared to the standard SAM, SAM-CLUBB has been shown to generate good simulations with a 16 km horizontal grid spacing [*Larson et al*., 2012]. Also, an order of 10 km grid spacing will be routinely used for large-scale models in the foreseeable future. As a reference, two simulations with 30 and 150 m vertical grid spacings are performed without FIVE. These simulations are named DZ30 and DZ150, respectively. For simulations with FIVE, 30 m vertical grid spacing is used below 2 km and 150 m grid spacing is used above 2 km for VEP. A grid spacing of 150 m is used for the host model. Each FIVE simulation is named according to the process(es) computed on VEP; M, R, T, and W represent simulations with microphysics (including condensation/evaporation, collision-coalescence, as well as sedimentation), radiation, turbulence, and vertical advection (i.e., subsidence) in VEP, respectively. For example, MTW denotes that microphysics, turbulence, and subsidence are computed in VEP while radiation is computed in the host model. (There is no significance to the order of the processes as they appear in the acronym; processes are all calculated in accord with the host model timing.)

For this test, SAM was modified so that it can run as an SCM. We will show results obtained with FIVE used in the SCM, as well as 2-D regional model simulations.

3.3. Single-Column Model Simulations

A number of studies have suggested that high resolution is necessary for successful stratocumulus simulations due to the tight interaction between microphysics, radiation, and turbulence [e.g., *Stevens et al*., 2005; *Zhu et al*., 2005]. With SCM simulations, we examine how the computation of an assigned process at coarser resolution changes the outcome and identify the cause of the bias.

For the SCM setup, MRTW is equivalent to DZ30 because dynamics is specified. Figure 3 shows the results from MRTW, DZ150, MRT, MRW, MTW, and RTW. The simulation duration is 12 h. First, we note that DZ150 produces results significantly different from MRTW, pointing to the importance of higher vertical resolution. DZ150 underestimates cloud water path (CWP) and rainwater path (RWP) compared to MRTW because of its inability to sustain the sharp gradient near the cloud top and to deepen the boundary layer. Second, any case that computes on the host model grid vertical transport such as advection by subsidence (MRT), turbulence mixing (microscopic advection; MRW), and advection by fall velocity for cloud and rainwater (RTW) produces results similar to or worse than DZ150 in terms of CWP and RWP.

The result of MRT, which computes subsidence in the host model, is poorer than DZ150 due to excessive cloud-top entrainment (i.e., higher PBL depth than MRTW), resulting in warming and drying of the PBL. The result for MRW, which computes turbulence in the host model, is also poor for the current prototype FIVE for two reasons. First, it results in a particularly noisy profile in VEP, indicating that the turbulent tendency computed in the host model, and/or the interpolated tendency, is too weak to mix the variability developed in VEP. Without CLUBB as a small-scale smoother in VEP, there is nothing else to effectively smooth the fluctuation developed in VEP. Second, the PBL depth is underestimated, similar to DZ150. The error in the PBL height in both MRT and MRW is caused by the imbalance between subsidence (macroscopic) and entrainment (microscopic) advective tendencies, which are computed at different resolutions. When the advective tendency associated with subsidence, i.e., $w\frac{\partial\phi}{\partial z}$, is computed in the host model (MRT), it is underestimated due to less accurate estimation of the vertical gradient. Furthermore, the current tendency interpolation scheme is not able to reproduce a magnitude of the inflection point (as is the case for the subsidence tendency around the inversion) close enough to that of the original high-resolution profile when the layer-

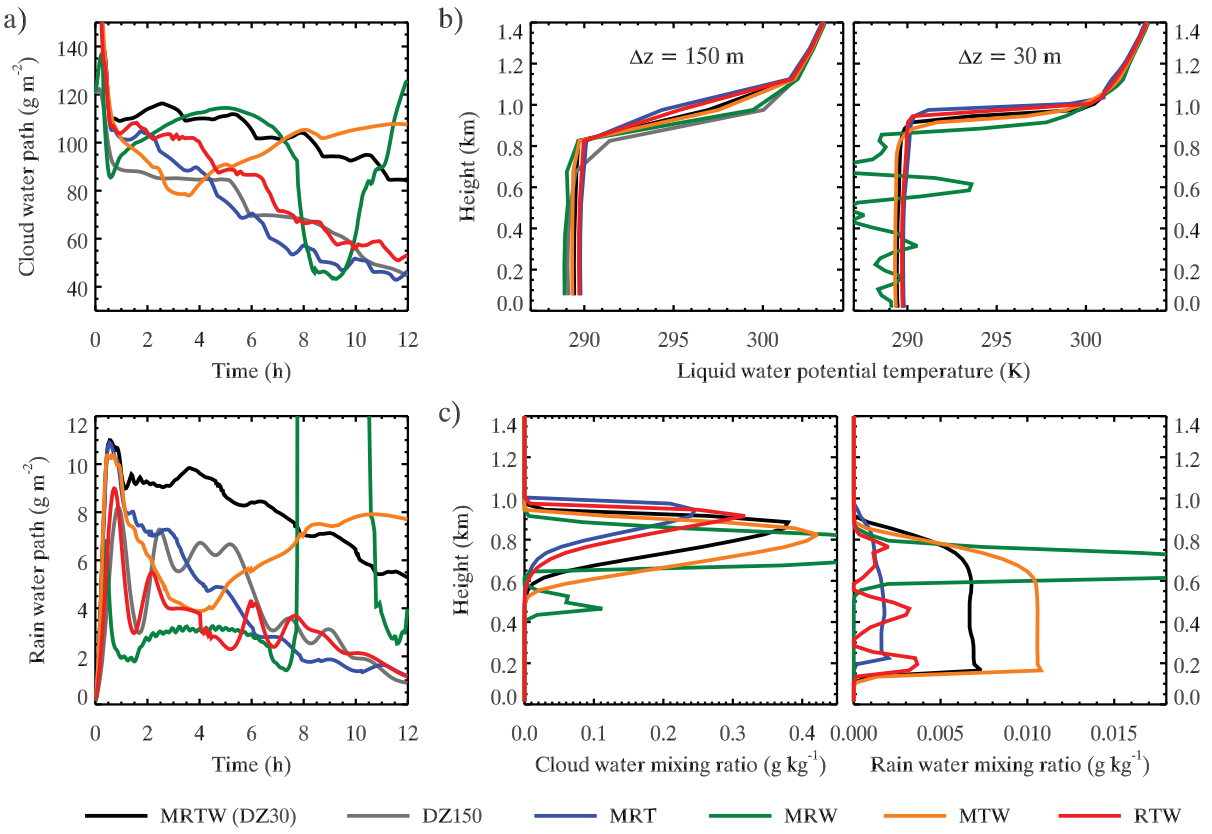

Figure 3. (a) Time series of cloud water path and rainwater path for MRTW, (equivalent to DZ30), DZ150, MRT, MRW, MTW, and RTW. (b) Profiles of these cases at 12 h for liquid water potential temperature. The vertical grid spacing for the left figure is 150 m (host model profiles for the FIVE simulations) and that for the right figure is 30 m (VEP profiles for the FIVE simulations). (c) VEP profiles for cloud water and rainwater mixing ratios at 12 h.

averaged profile is used as an input. The magnitude of inflection is either under or overestimated depending on the shape of tendency profile, and for subsidence, the tendency is underestimated at the PBL top. Since the subsidence tendency is weaker, it is too weak to balance turbulence entrainment as in the case of MRTW, hence it results in a higher PBL height than MRTW. When turbulence is computed in the host model (MRW), the tendency associated with turbulence mixing is underestimated, which results in lower PBL height than MRTW. These results suggest that any process associated with vertical transport is key and should be computed in VEP.

The result of RTW, which computes microphysics in the host model, shows that microphysics needs to be processed in VEP since it includes vertical transport in the form of cloud water sedimentation and rainwater precipitation. Our analysis suggests that the bias associated with sedimentation produces higher PBL depth, which results in a warmer PBL by entrainment, and the bias associated with precipitation results in very noisy rainwater mixing ratio profiles.

The result for MTW, which computes radiation in the host model, neither continuously reduces both CWP and RWP nor creates noisy profiles in VEP. MTW oscillates with larger amplitude than MRTW, but tracks MRTW quite well. The source of the differences between MTW and MRTW is analyzed next.

Three-day simulations for MRTW and MTW are performed to see if MTW indeed exhibits oscillations in CWP but follows MRTW, and to understand the cause of the oscillations. Figure 4a clearly shows that MTW oscillates with larger amplitude than MRTW, but follows it reasonably well. The cause of this oscillation is the inability of the current tendency interpolation scheme to accurately capture the longwave heating rate at the cloud top. The current tendency interpolation scheme shares the location of local inflection points, such as the maximum longwave cooling rate shown in Figure 4b, between the host model and VEP. Thus, when the longwave heating rate is interpolated to the VEP level, the maximum cooling is often applied not to the cloud top, but rather below or above the cloud top. As shown in Figure 4a, when the PBL height of the host

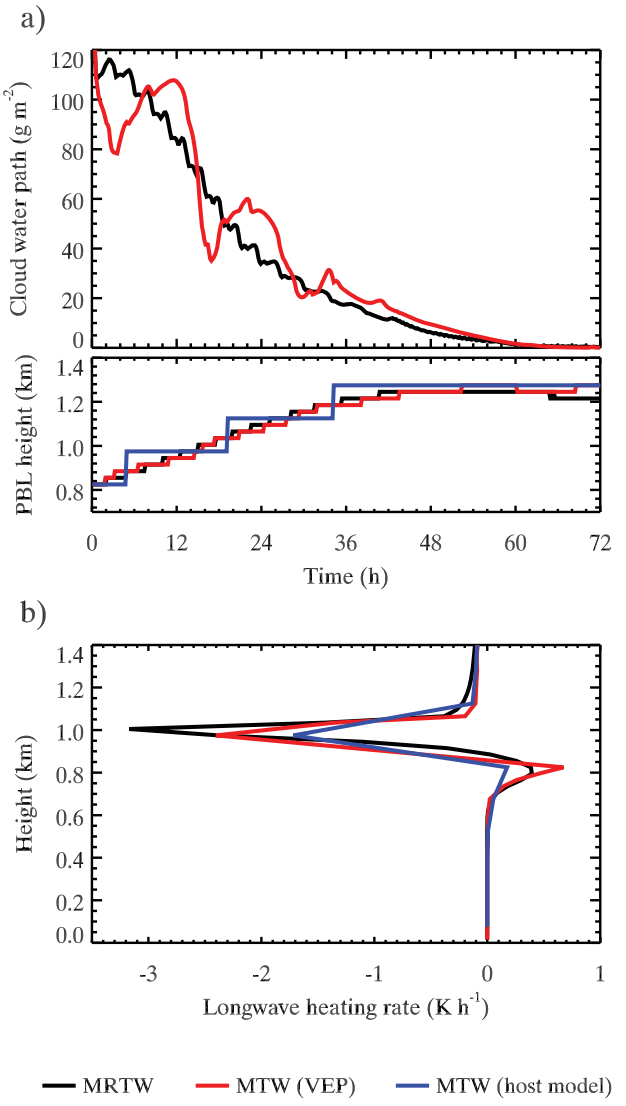

Figure 4. Results for a 3 day simulation of MRTW and MTW; (a) time series of CWP and PBL height and (b) profile of longwave heating rate at 18 h where CWP of MTW is smaller than MRTW, and the PBL height of the host model is lower than that of VEP. The VEP profile for MTW (red) is interpolated from the host model profile (blue).

model for MTW rises by one level, CWP increases because the longwave cooling is applied above the cloud top region, which promotes more condensation; in contrast, CWP decreases when the PBL height in VEP is higher than that of the host model because the longwave cooling is applied below the cloud top, and entrainment effectively dries the cloud.

The artificial oscillation discussed above can be effectively circumvented with the local vertical mesh refinement described in section 2.2. As illustrated in Figure 2, FIVE's local vertical mesh refinement creates a local high-resolution profile around the cloud top by inserting a portion of the profile of VEP into the host model profile and computes a process with the prepared local high-resolution profiles. A new case, MR_LTW, uses this local vertical mesh refinement method for radiation. Figure 5 shows that results for MRTW and MR_LTW are nearly identical.

The SCM simulations for the prototype FIVE show that

1. CLUBB must be used in VEP as a small-scale smoother. This is likely true for other turbulence parameterizations.
2. Vertical transport such as subsidence and sedimentation/precipitation should be computed in VEP.
3. Radiation may be computed outside VEP provided that a method which effectively removes the artificial oscillation is used. The local vertical mesh refinement method applied for radiation gives very good results.

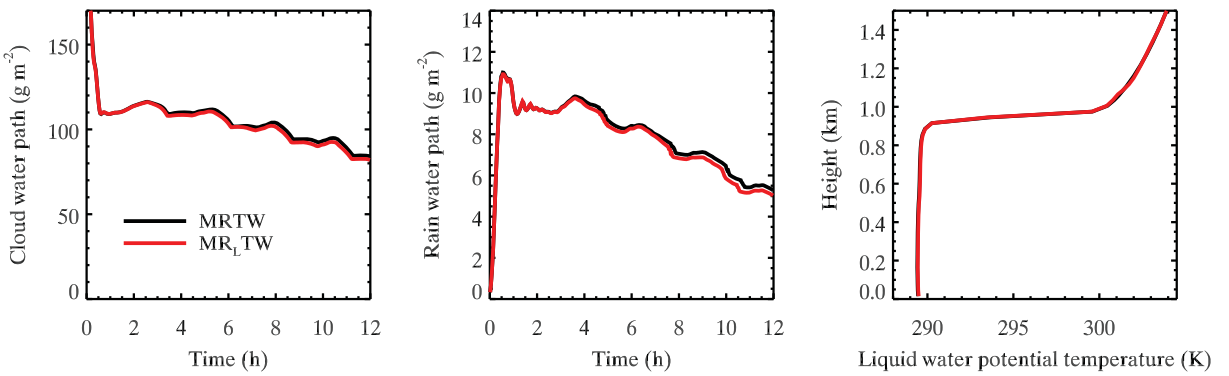

Figure 5. Results with the local vertical mesh refinement method applied to radiation (MR_LTW) and MRTW. CWP, RWP, and the profile of liquid water potential temperature at 12 h are shown.

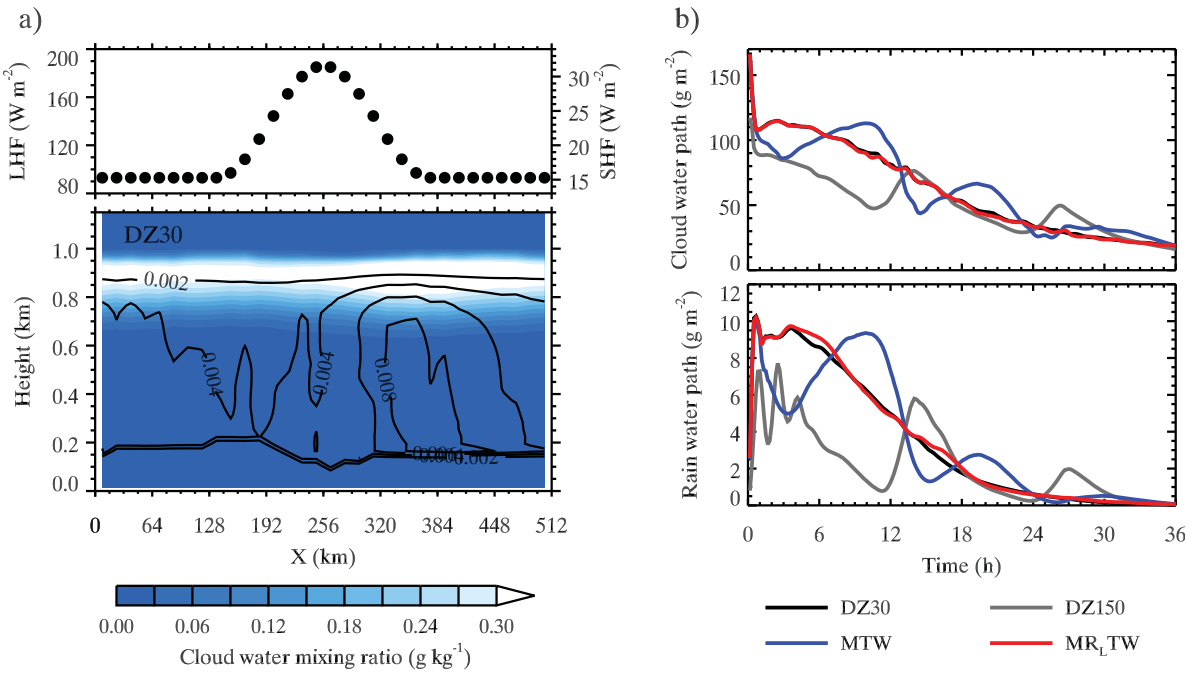

Figure 6. (a) The upper figure shows the modified prescribed surface fluxes for sensible and latent heat (SHF and LHF, respectively), and the lower figure shows the cloud water mixing ratio (filled contour) and rainwater mixing ratio (black contour line, every 0.002 g kg^{-1}) for DZ30 at 13 h. The direction of the horizontal velocity is from left to right. (b) Time series of domain mean cloud water path and rainwater path for DZ30, DZ150, MTW, and MR$_L$TW.

4. The tendency interpolation scheme has room for improvement regarding location and magnitude of inflection points.

3.4. Two-Dimensional Regional Simulations

FIVE is now tested for a 2-D simulation of the same case in order to explore the capability of FIVE's tendency interpolation scheme to represent the horizontal advective tendency in VEP when horizontal gradients develop in the host model.

The number of horizontal grid points is 32, thus the horizontal domain size is 512 km (i.e., 16 km horizontal grid spacing). The lateral boundary condition is periodic. The simulation duration is 36 h. In order to generate horizontal gradients for a 2-D domain, a warm pool (i.e., increased sensible and latent heat fluxes, Figure 6a) is placed in the domain center. In addition, the zonal wind speed is increased from 3 to 10 m s^{-1} at the surface, which changes it from approximately 6.4 to 13.4 m s^{-1} at the initial inversion height (800 m), which means that the cloudy air travels a horizontal distance roughly 3 times as long as the domain size over 36 h. The other model configurations are the same as the SCM tests. We run DZ30, DZ150, MTW, and MR$_L$TW. Figure 6a shows the specified surface fluxes and cloud and rainwater fields at 13 h for DZ30. During the simulations, resolved-scale vertical velocity with a maximum of approximately 7 mm s^{-1} develops within the PBL. For the W option in the prototype FIVE, subsidence is processed in VEP but advection by resolved-scale vertical velocity is processed in the host model. Further development is necessary to compute advection by the resolved-scale vertical velocity in VEP. In any case, its effect is minor for the current case.

Figure 6b shows the domain mean CWP and RWP. MR$_L$TW agrees very well with DZ30. As expected, MTW gives oscillatory results around DZ30. The strong agreement between MR$_L$TW and DZ30 comes from accurately predicted fields. Figure 7 presents Taylor diagrams [*Taylor*, 2001] for cloud water and rainwater mixing ratios. The profiles at 13 h are used for this analysis since both CWP and RWP are similar among the cases. Correlation, standard deviation, and root-mean-square differences are computed for each column profile below 1.3 km by comparing to the profile of DZ30. In the figure, each column is represented by filled circles for the VEP profiles of MTW and MR$_L$TW. The profile of DZ30 averaged to the 150 m grid spacing is used to compute statistical quantities for DZ150 and the host model of MTW and MR$_L$TW, and each column is represented with open circles. For each column, standard deviations and root-mean-square differences

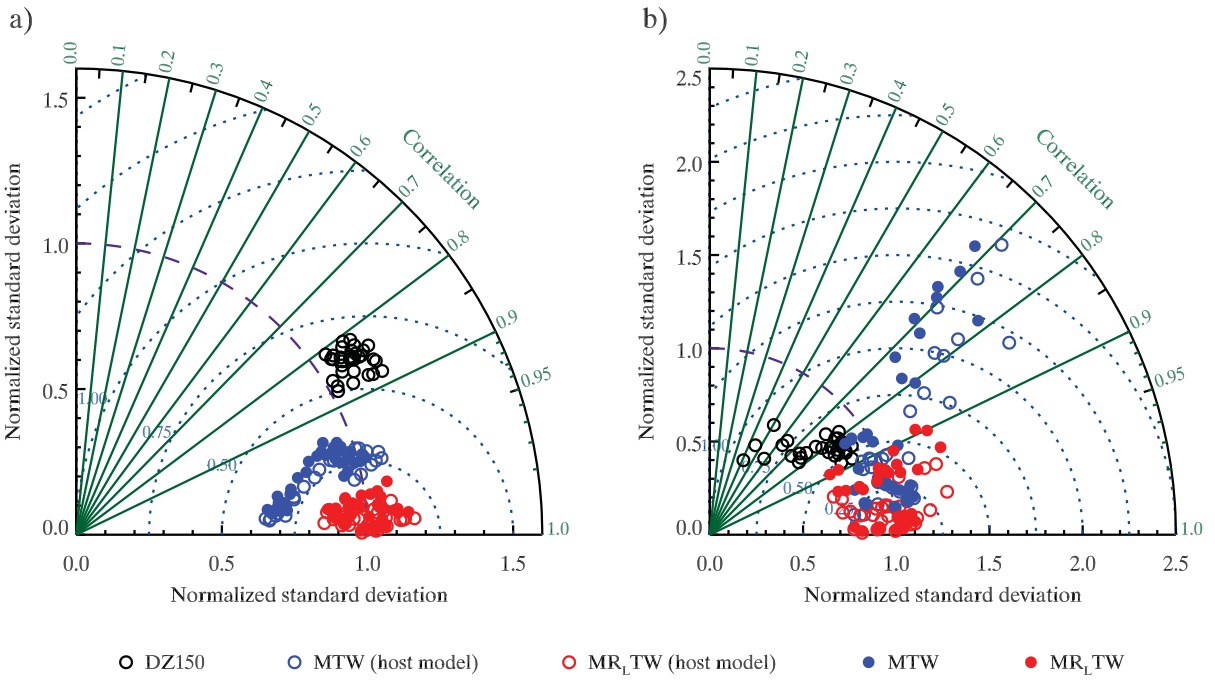

Figure 7. Taylor diagram of (a) cloud water profile and (b) rainwater profile below 1.3 km for every column in the domain relative to DZ30 for DZ150, MTW, and MR_LTW at 13 h. Standard deviations and root-mean-square differences (blue dotted line) are normalized. The open circles represent the 150 m grid spacing while the filled circles represent the 30 m grid spacing.

(blue dotted lines) have been normalized in order to fit all columns in one panel. A correlation of 1 and a normalized standard deviation of 1 mean an exact match of a column profile to DZ30.

In the Taylor diagrams, for the profiles defined on 150 m grid spacing (host model for the FIVE simulations; open circles), MR_LTW maintains correlations close to 1 for the entire domain after 13 h, even for most of the rainwater profiles. For MR_LTW, normalized standard deviations are clustered around 1, and the root-mean-square difference is smallest. Thus, MR_LTW successfully reproduces the DZ30 profiles. MTW also retains high correlation for both cloud water and rainwater, but the bias for rainwater is larger than MR_LTW, while DZ150 has the largest bias in the correlation of rainwater. The ranges of normalized standard deviation for MTW are larger than those of DZ150 for both variables. MTW also has columns with larger root-mean-square differences compared with DZ150. MTW is anticipated to follow DZ30 with an amplified oscillation for CWP and RWP, while DZ150 has diverged from DZ30 for CWP and RWP from the beginning. The fact that DZ150 has similar CWP and RWP to DZ30 is a result of offsetting of errors associated with incorrect profiles. For the MR_LTW and MTW VEP profiles, the correlation becomes slightly smaller than that on the host model grid.

The 2-D simulations suggest that computing momentum and horizontal scalar advection on the host model coarse vertical grid does not degrade the overall result significantly. One might be tempted to conclude that cost savings could be achieved by solving the vertical transport equations at high resolution, and the momentum and horizontal scalar advection at coarse resolution. However, given the idealized nature of the 2-D simulations, this conclusion is premature and will have to be reevaluated in large-scale models where the circulation can be perturbed at a range of spatiotemporal scales.

4. Beyond the Prototype FIVE

The prototype FIVE shows the great benefit of using high vertical resolution for turbulence, subsidence, and microphysics to represent the stratocumulus-capped PBL. FIVE gives comparable results to its high-resolution reference simulation and provides confidence that the framework will likely improve representation of low clouds in large-scale models. However, a number of developments are necessary in order for FIVE to be used operationally. In addition, even though it is much less expensive than MMF, it is desirable to reduce numerical costs associated with FIVE. In this section, we will discuss these further developments as well as ideas to mitigate numerical costs associated with FIVE, while retaining overall accuracy.

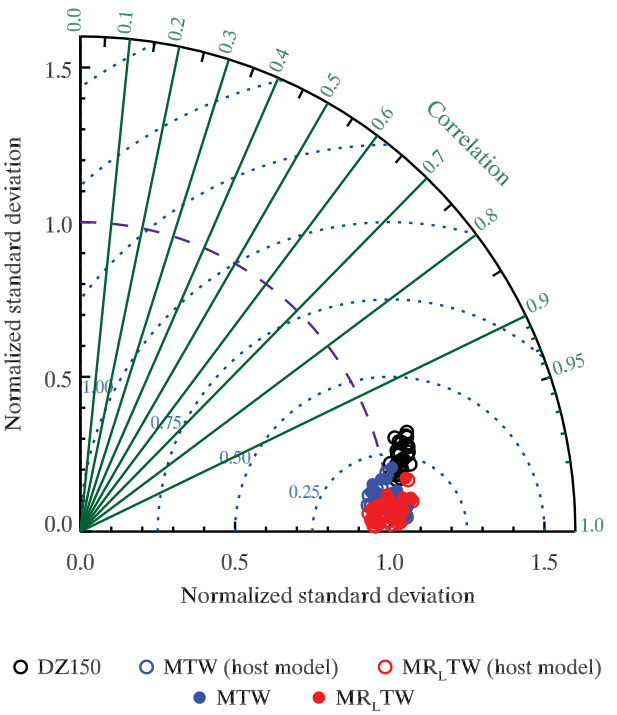

Figure 8. Same as Figure 7 but for zonal velocity.

4.1. Horizontal Velocity in VEP

In the prototype FIVE, subsidence is applied to $\mathbf{U}_H$ but not to $\mathbf{u}_H$; thus, only turbulent diffusion is computed for $\mathbf{u}_H$. Our analysis suggests that predicting $\mathbf{u}_H$ may be unnecessary. As shown in Figure 8, the horizontal velocity predicted for DZ150, the low-resolution reference simulation, is marginally degraded compared with FIVE simulations. Instead of predicting $\mathbf{u}_H$, an interpolated horizontal velocity from $\mathbf{U}_H$ to compute turbulence tendency in VEP may suffice.

4.2. Use of the High-Resolution Profile for Tendency Interpolation

There is room for improvement of the tendency interpolation scheme. The scheme could potentially be tailored for specific processes based on physical knowledge and information from VEP.

We have shown that FIVE's current tendency interpolation scheme cannot capture the appropriate height for the maximum longwave cooling in the VEP level, which is the source of the amplified oscillation observed in CWP and RWP. This could be improved with use of the cloud water profile on the high-resolution level. The local maximum (minimum) of longwave cooling as well as shortwave warming are generally located very close to the level of the local maximum (minimum) of cloud water content. For instance, within each host model layer that has an inflection point in the radiative heating rate, the level of the inflection point for the cloud water content in VEP could be matched with the level of the heating rate inflection for the purpose of interpolation. This modification is expected to reduce the amplitude of the oscillation in CWP and RWP. This method should be less expensive than the local vertical mesh refinement method.

As mentioned in section 3.3, the current scheme underestimates the magnitude of the inflection. Because of the use of a linear function (Appendix B), the scheme is not good at representing discontinuities, which leads to underestimation/overestimation of the inflection value (Figure 4b). It should be possible to adjust the magnitude of the inflection, based on the high-resolution profile in VEP.

4.3. Advection by Vertical Velocity

In the prototype FIVE, advection by the resolved-scale vertical velocity is always computed in the host model while advection by large-scale vertical velocity, i.e., subsidence, is computed in VEP. This separation of vertical velocity is done merely as an expedient treatment for stratocumulus PBLs for 2-D simulation. There is no separation between resolved-scale velocity and subsidence for large-scale models; thus, the vertical advection scheme has to be implemented into VEP to balance turbulence mixing at the stratocumulus top.

For models built with a time splitting advection scheme in horizontal and vertical directions, it is relatively easy to port the vertical advection scheme into VEP. Three-dimensional advection schemes often use an operator splitting method, which computes the advective tendency for each direction separately. In this case, one could separate vertical advection from horizontal advection. A concern is that numerical diffusion may become larger due to double application of a monotonic limiter to scalars. Also, the credibility of the linear interpolation for vertical velocity to the VEP levels may need to be evaluated.

Once the vertical advection is separated, the following two options would be worth exploring: local vertical mesh refinement as well as use of a local PBL top for the advective tendency interpolation. It should be

noted that if FIVE is applied to chemical tracers, the cost for vertical advection in VEP could become significant and should be used judiciously.

For radiation calculations, FIVE's local vertical mesh refinement at cloud top produces good results. This method would also be useful for vertical advection. Our tests show that accurate vertical transport associated with subsidence that balances turbulence mixing is key to maintaining stratocumulus cloud. Thus, application of the local vertical mesh refinement around the PBL top to vertical advection is likely to reduce cost while retaining accurate evolution of the PBL.

For weak vertical velocity at the PBL top, the advective tendency is anticipated to be large where the vertical gradient is large. A similar strategy outlined above for the radiative heating would be applicable for vertical advection; using the local PBL top, the interpolation scheme could be guided to output a better profile of the vertical advective tendency.

4.4. Adaptive Vertical Grid for VEP

The total cost of running a GCM with FIVE is anticipated to be less than running the entire GCM at high vertical resolution, and much less than MMF. (MMF with 64 grid columns in the embedded CSRM requires a factor of about 200 times more computation time than a conventional GCM [*Khairoutdinov et al*., 2005].) Since the cost associated with FIVE is tightly related to the number of VEP levels, the VEP cost burden could be reduced by applying an Adaptive Vertical Grid (AVG) method [*Marchand and Ackerman*, 2010] to the VEP grid. With AVG, the vertical extent of the vertical enhancement, as well as the degree (i.e., grid spacing) of vertical enhancement of the VEP levels, is adjusted dynamically. (The VEP time step for sub-time stepping will be adjusted according to the adjusted resolution.)

Since the depth of the boundary layer ranges from a few hundred meters to several kilometers, it is wasteful to use high resolution up to, for example, 5 km when a PBL top is at 1 km. Besides, VEP likely requires fine grid spacing for stratocumulus, but it may not require fine grid spacing for shallow cumulus where temperature and humidity gradients in the inversion are weaker. In addition, there could be PBL states that are reasonably well represented by the coarser resolution used in the large-scale host model. Thus, the degree of vertical enhancement (resolution) should depend on the PBL state.

With a successful AVG, when the PBL is characterized as stratocumulus-capped, the VEP vertical resolution will become fine and the vertical extent will be set. When the PBL state becomes shallow cumulus-like, the vertical resolution will become gradually coarser, and the vertical extent will increase. When the PBL state is cloud-free then the VEP levels will default to the host model levels. *Marchand and Ackerman* [2010] tested an AVG method for shallow clouds with 2-D near-LES (100 m horizontal grid) and showed successful results, providing independent evidence for improvements that can be realized by AVG/VEP.

Since AVG is applied to every column for VEP, it may result in great variability in the number of VEP levels over the domain. Parallel computing is costly when cores are idle while waiting for cores with the longest computation time. Thus for parallel computing, the application of AVG alone would not reduce the net computational cost. For effective parallelization, the cost should ideally be the same for all cores; that is, imbalanced costs among the cores not only waste resources due to the creation of idling cores but also reduce accuracy because those idling cores use lower VEP resolution. There is, however, a workaround in the form of "work stealing" [*Blumofe and Leiserson*, 1999; *Yang and He*, 2017]. In this method, a core "steals" some of the other cores' work when it runs out of work. Work stealing can be implemented for internode as well as intranode calculations. Work stealing would maximize the compatibility between AVG and parallelization.

5. Summary and Conclusions

We have presented a new framework for improving the representation of low and (potentially) high clouds in large-scale models such as GCM, MMF, and CSRM, focusing on vertical resolution as a cause of biases in simulated clouds. FIVE embeds VEP, which uses the same physical parameterizations of turbulence, convection, microphysics, and vertical advection solved in the coarse-grid, large-scale host model. VEP is implemented on a locally high vertical resolution grid in the PBL and, in the case of cirrus, near the tropopause. Each process calculation in VEP is called at the same point in time when the host model would otherwise compute it. Thus, there is no modification to the model algorithm in order to implement FIVE. The host

model and VEP are synchronized by exchanging tendencies with each other to prevent any drift in the host model state.

A prototype of FIVE is used to demonstrate that SCM and regional model simulations of a drizzling stratocumulus-capped PBL are significantly improved when the physics is solved at higher vertical resolution. The framework also allows one to evaluate the error associated with solving different subsets of the physics at lower resolution and provides possible ways to overcome the error without the use of high resolution. For the case under discussion, it is shown using SCM simulations that the higher-order closure scheme used here (CLUBB) must be computed on the high-resolution vertical mesh. This is probably true for other turbulence parameterizations. Vertical transport such as subsidence and sedimentation/precipitation should also be computed in VEP. On the other hand, when radiation is computed in the host model, simulations exhibit a low-frequency oscillation around the high-resolution solution. This artificial oscillation can be effectively avoided using a local vertical mesh refinement (Figure 2). Experiments with a local vertical mesh refinement method applied for radiation in the vicinity of the PBL top produce superior results (Figure 5).

One of the distinct advantages of FIVE is that it is a computational framework, which means that it is not tied to a specific physical parameterization. Thus, it will work with any parameterization for turbulence, convection, microphysics, and radiation. It is expected to perform best in combination with parameterizations that demonstrate clear improvement in results with enhanced vertical resolution.

FIVE is still in its infancy and requires further refinement and testing (section 4). We have identified a path forward for application in large-scale models and considered ways in which the cost-benefit ratio can be reduced. Future work will test these ideas more broadly, i.e., for different PBL, cloud regimes, and cirrus clouds.

Appendix A: FIVE for a Compressible System

Models formulated for a compressible system often predict mass-weighted quantities, e.g., $\rho\phi$. In this case, the host model layer mean of $\rho\phi$ is written as

$$(R\Phi)_K = \overline{\rho\phi}_K = \frac{1}{\Delta Z_K}\sum_{i=k-n}^{k+n}(\phi\rho\delta z)_i\,. \tag{A1}$$

The host model tendency for the synchronization of VEP is written as

$$\partial_t(R\Phi)_K^{n*} = \frac{(R\Phi)_K^{n*} - \overline{\rho\phi}_K^{n}}{\Delta t}\,. \tag{A2}$$

As described in Appendix B, since our tendency interpolation scheme interpolates mass-weighted tendency, there is no need to modify the interpolation scheme. $\rho\phi$ is updated by

$$(\rho\phi)_k^{n*} = (\rho\phi)_k^{n} + \Delta t \cdot \text{interpolation}\left[\partial_t(R\Phi)^{n*}\right]. \tag{A3}$$

After updating $(\rho\phi)_k^{n*}$ to $(\rho\phi)_k^{n**}$ in VEP, the synchronization of the host model to VEP is performed with

$$\overline{\partial_t(\rho\phi)}_K^{n**} = \frac{\overline{\rho\phi}_K^{n**} - (R\Phi)_K^{n*}}{\Delta t}\,. \tag{A4}$$

Since R is predicted, ρ has to be updated. A simple way to predict ρ is as follows. When R_K^n is fully updated to R_K^{n+1}, ρ_k^n is updated as

$$\rho_k^{n+1} = \rho_k^n + \text{interpolation}\left(R_K^{n+1} - \bar{\rho}_K^n\right). \tag{A5}$$

When the density change is expected to be small over one time step, this method should suffice. How detailed a treatment for predicting ρ is necessary remains to be examined.

Appendix B: Interpolation Scheme for the Host Model Tendency

Our interpolation scheme first obtains an estimation on the VEP grid with the interpolation scheme of *Sheng and Zwiers* [1998, hereafter SZ98], and then applies a monotonic filter where the method of *Zerroukat et al*. [2005, hereafter ZWS05] detects a violation of monotonicity.

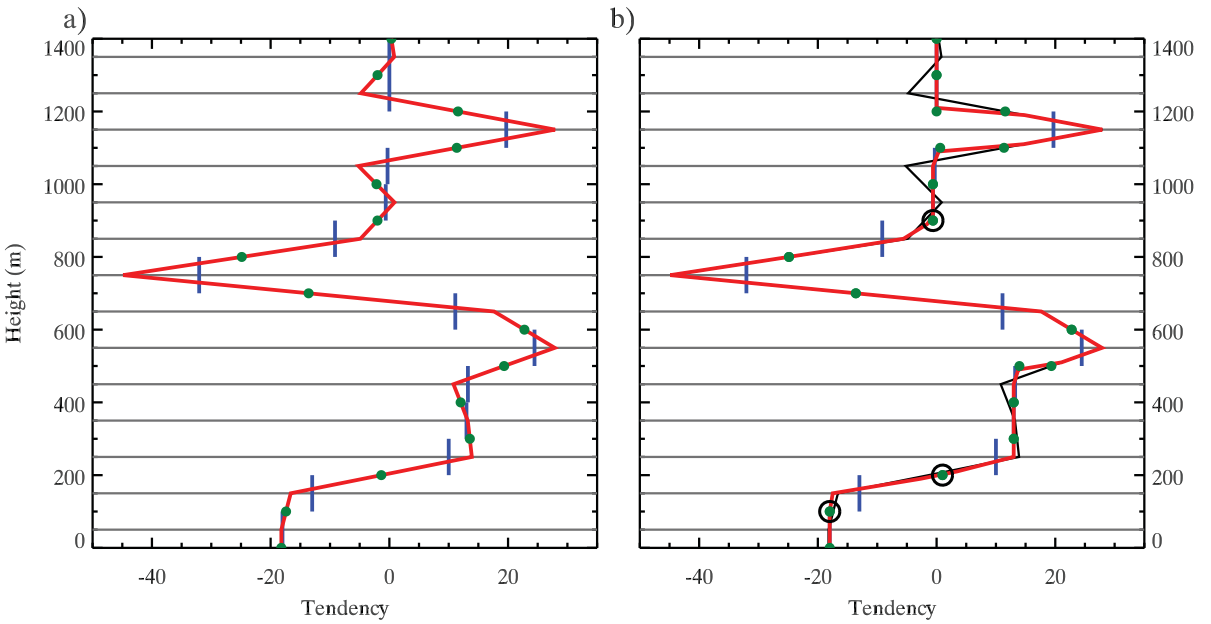

Figure B1. Example for interpolation of a hypothetical host model tendency (blue): (a) interpolated profile (red) and the estimated interface values (green circles) obtained with the base interpolation method of *Sheng and Zwiers* [1998]; (b) interpolated profile (red) constructed with the interface values (green circles) adjusted with a new monotonic filter. The interface value after removal of discontinuities is indicated with a black circle. The profile is superimposed on the nonadjusted profile (black). The height of each value of the host model tendency (blue) is equal to the host model grid spacing (100 m), and the gray horizontal lines are located at Z_K.

B1. The SZ98 Interpolation Scheme

The interpolation scheme of SZ98 breaks the interpolated profile into linear segments between two local target values. Each local target value is located within its host model layer, and typically at the Z level where the corresponding mean value is located, although this is not necessary as long as it lies within the host model layer. These local target values are obtained by solving a system of equations for the target values, which is a result of enforcing conservation of the average of the scalar, i.e., $\overline{\partial_t \phi}_K = \partial_t \Phi_K$, for all K. The system of equations is written as

$$\mathrm{M}\psi_{\odot} = \Psi\,, \tag{B1}$$

where M is the matrix of coefficients, the subscript $\odot$ represents the target value, and

$$\psi \equiv \rho \partial_t \phi\,, \tag{B2a}$$

$$\Psi \equiv R \partial_t \Phi\,. \tag{B2b}$$

Both $\psi_{\odot}$ and Ψ are 1-D vectors with size equal to the number of host model levels. The system of equations is characterized by a tri-diagonal matrix because Ψ_K is a weighted sum of $\psi_{\odot,K-1}$, $\psi_{\odot,K}$, and $\psi_{\odot,K+1}$. The solution to M is therefore very efficient. It should be noted that the target value becomes a local inflection point when the host model layer is an inflection point. As discussed in section 4.2, the local inflection point is assigned to the appropriate VEP level within the layer.

B2. Detecting and Correcting Nonmonotonicity

The SZ98 scheme sometimes creates a spurious shape in the constructed high-resolution profile where the profile on the host model level is locally monotonic (Figure B1a). Our scheme utilizes the method of ZWS05, which detects the violation of local monotonicity and corrects it by adjusting one of two estimated *interface* values on $\hat{Z}$.

In our scheme, the interface value is computed from the target values obtained with the SZ98 scheme. Recall that the host model and VEP levels conform to the following relationship:

$$\ldots < \begin{bmatrix} \hat{Z}_K \\ \hat{z}_{k-n} \end{bmatrix} < z_{k-n} < \ldots < \hat{z}_k < \begin{bmatrix} Z_K \\ z_k \end{bmatrix} < \hat{z}_{k+1} < \ldots < z_{k+n} < \begin{bmatrix} \hat{Z}_{K+1} \\ \hat{z}_{k+n+1} \end{bmatrix} < \ldots . \tag{B3}$$

The interface value at $\hat{Z}_K$ is computed by linearly interpolating two adjacent target values as

$$\hat{\psi}_K = \frac{z_{\odot,K} - \hat{Z}_K}{z_{\odot,K} - z_{\odot,K-1}} \psi_{\odot,K-1} + \frac{\hat{Z}_K - z_{\odot,K-1}}{z_{\odot,K} - z_{\odot,K-1}} \psi_{\odot,K}, \tag{B4}$$

where $z_{\odot,K}$ denotes the level of the target value. For simplicity, $\hat{\psi}_1 = \psi_{\odot,1}$.

The method of ZWS05 is summarized as follows. Spurious violation is detected with the condition of

$$\left(\hat{\psi}_K - \Psi_{K-1}\right)\left(\Psi_K - \hat{\psi}_K\right) > 0\,, \tag{B5}$$

and any of the conditions below

$$(\Psi_{K-1} - \Psi_{K-2})(\Psi_{K+1} - \Psi_K) \geq 0\,, \tag{B6a}$$

$$(\Psi_{K-1} - \Psi_{K-2})(\Psi_{K-2} - \Psi_{K-3}) \leq 0\,, \tag{B6b}$$

$$(\Psi_{K+1} - \Psi_K)(\Psi_{K+2} - \Psi_{K+1}) \leq 0\,, \tag{B6c}$$

$$\left(\hat{\psi}_K - \Psi_{K-1}\right)(\Psi_{K-1} - \Psi_{K-2}) \leq 0\,. \tag{B6d}$$

This set of conditions is able to detect the violation for interface values estimated with any degree of the polynomial. For monotonicity, the interface value has to be bounded between Ψ_{K-1} and Ψ_K. The spurious interface value is then modified as

$$\hat{\psi}_K = \alpha \Psi_{K-1} + (1-\alpha)\Psi_K\,, \tag{B7}$$

where

$$\alpha = H\left(|\hat{\psi}_K - \Psi_K| - |\hat{\psi}_K - \Psi_{K-1}|\right) \tag{B8}$$

is a Heaviside step-function where $H(x)=1$ when $x \geq 0$ and $H(x)=0$ when $x<0$.

B3. Adjustment of the Target Value Based on the Corrected Interface Values

The target value has to be modified when one or two adjacent interface layers are corrected with the ZWS05 method so that the interpolated profile passes through the interface values as well as the target value, all the while ensuring that the conservation requirement is fulfilled. These properties are also true for our base interpolation method (B1).

We consider linear interpolation between $\hat{\psi}_K$ and $\psi_{\odot,K}$ to the VEP levels between $\hat{Z}_K$ and $z_{\odot,K}$, as well as with $\psi_{\odot,K}$ and $\hat{\psi}_{K+1}$ to the VEP levels between $z_{\odot,K}$ and $\hat{Z}_{K+1}$ so that

$$\psi_i = (1-\omega_i)\hat{\psi}_K + \omega_i \psi_{\odot,K} \text{ for } \hat{Z}_K < z_i \leq z_{\odot,K}\,, \tag{B9a}$$

$$\psi_i = (1-\omega_i)\hat{\psi}_{K+1} + \omega_i \psi_{\odot,K} \text{ for } z_{\odot,K} \leq z_i < \hat{Z}_{K+1}\,, \tag{B9b}$$

where

$$\omega_i = \frac{z_i - \hat{Z}_K}{z_{\odot,K} - \hat{Z}_K} \text{ for } \hat{Z}_K < z_i \leq z_{\odot,K}\,, \tag{B10a}$$

$$\omega_i = \frac{z_i - \hat{Z}_{K+1}}{z_{\odot,K} - \hat{Z}_{K+1}} \text{ for } z_{\odot,K} \leq z_i < \hat{Z}_{K+1}\,. \tag{B10b}$$

The interpolation with (B9) satisfies the conservation when the target value obtained from the SZ98 method (B1) and the interface values estimated with (B4) are used.

With the linear function assumption, the conservation relationship can be written as

$$c_0\Psi_K = c_1\psi_{\odot,K} + c_2\hat{\psi}_K + c_3\hat{\psi}_{K+1}\,, \tag{B11}$$

where

$$c_0 = 2c_1\,, \tag{B12a}$$

$$c_1 = \hat{Z}_{K+1} - \hat{Z}_K\,, \tag{B12b}$$

$$c_2 = z_{\odot,K} - \hat{Z}_K\,, \tag{B12c}$$

$$c_3 = \hat{Z}_{K+1} - z_{\odot,K}\,. \tag{B12d}$$

Thus, the target value is adjusted with the corrected interface values and the average value by

$$\psi_{\odot,K} = \frac{1}{c_1}\left(c_0\Psi_K - c_2\hat{\psi}_K - c_3\hat{\psi}_{K+1}\right). \tag{B13}$$

B4. Ensuring Monotonicity

The resultant profile may still be nonmonotonic within a local monotonic layer. This stems from the inability of the linear function to meet the conservation without forming an inflection at the location of the target value. This could be avoided with a higher-order polynomial interpolation. We fix this problem by correcting the target value and one of the interface values.

The violation of local monotonicity is detected with the following two conditions

$$(\Psi_K - \Psi_{K-1})(\Psi_{K+1} - \Psi_K) \geq 0\,, \tag{B14a}$$

$$\left(\psi_{\odot,K} - \hat{\psi}_K\right)\left(\hat{\psi}_{K+1} - \psi_{\odot,K}\right) < 0\,. \tag{B14b}$$

When both conditions are met, the interpolated profile is spurious and the target value is corrected by applying

$$\psi_{\odot,K} = \beta\hat{\psi}_{K+1} + (1-\beta)\hat{\psi}_K\,, \tag{B15}$$

where

$$\beta = H\left(|\psi_{\odot,K} - \hat{\psi}_K| - |\psi_{\odot,K} - \hat{\psi}_{K+1}|\right). \tag{B16}$$

This procedure sets $\psi_{\odot,K}$ to either $\hat{\psi}_K$ or $\hat{\psi}_{K+1}$. When $\beta = 1$, $\psi_{\odot,K} = \hat{\psi}_{K+1}$, and $\hat{\psi}_K$ is given as

$$\hat{\psi}_K = \frac{1}{c_2}\left(c_0\Psi_K - c_1\psi_{\odot,K} - c_3\hat{\psi}_{K+1}\right). \tag{B17}$$

This correction is applied for each host model layer and thus may create a discontinuity at the host model interface level, resulting in two interface values for the host model layer above and/or below. As shown in Figure B1b, however, the result is a more preferable shape. Now the interpolated profile is monotonic for a host model layer with a monotonic profile.

B5. Removal of Discontinuities

The last procedure is the removal of discontinuities at the interface levels as many times as possible. This adjustment is performed to all host model layers with monotonic profiles, which now can be identified with $(\psi_{\odot,K} - \hat{\psi}_K)(\hat{\psi}_{K+1} - \psi_{\odot,K}) \geq 0$, by removing one of the two interface values at the discontinuity whenever possible. This procedure is started from the lowest host model layer and continues upward.

For the monotonic profile layers, $\psi_{\odot,K}$ is computed again with (B11) as

$$\psi_{\odot,K} = \frac{1}{c_1}\left(c_0\Psi_K - c_2\hat{\psi}_K^{\text{below}} - c_3\hat{\psi}_{K+1}^{\text{above}}\right), \tag{B18}$$

where $\hat{\psi}_K^{\text{below}}$ is the upper interface level value for Z_{K-1} and $\hat{\psi}_{K+1}^{\text{above}}$ is the lower interface level value for Z_{K+1}. When

$$\left(\psi_{\odot,K}-\hat{\psi}_K^{\text{below}}\right)\left(\hat{\psi}_{K+1}^{\text{above}}-\psi_{\odot,K}\right)\geq 0 \tag{B19}$$

is met, $\psi_{\odot,K}$ is bounded between $\hat{\psi}_K^{\text{below}}$ and $\hat{\psi}_{K+1}^{\text{above}}$, and the procedure is to set $\hat{\psi}_K=\hat{\psi}_K^{\text{below}}$ and $\hat{\psi}_{K+1}=\hat{\psi}_{K+1}^{\text{above}}$, and then to proceed to the next level. If the condition is not satisfied, $\psi_{\odot,K}$ is modified by

$$\psi_{\odot,K}=\gamma\hat{\psi}_{K+1}^{\text{above}}+(1-\gamma)\hat{\psi}_K^{\text{below}}, \tag{B20}$$

where

$$\gamma=H\left(|\psi_{\odot,K}-\hat{\psi}_K^{\text{below}}|-|\psi_{\odot,K}-\hat{\psi}_{K+1}^{\text{above}}|\right). \tag{B21}$$

When $\gamma=0$, $\psi_{\odot,K}=\hat{\psi}_K^{\text{below}}$, $\hat{\psi}_K$ is set to $\hat{\psi}_K^{\text{below}}$, and $\hat{\psi}_{K+1}$ is given as

$$\hat{\psi}_{K+1}=\frac{1}{c_3}\left(c_0\Psi_K-c_1\psi_{\odot,K}-c_2\hat{\psi}_K\right). \tag{B22}$$

The new set of $\psi_{\odot,K}$, $\hat{\psi}_K$, and $\hat{\psi}_{K+1}$ will not create an inflection. For example, when $\psi_{\odot,K}$ obtained from (B18) is such that $\psi_{\odot,K}\leq\hat{\psi}_K^{\text{below}}<\hat{\psi}_{K+1}^{\text{above}}$, the procedure will result in $\psi_{\odot,K}=\hat{\psi}_K=\hat{\psi}_K^{\text{below}}$. For this example, it is true that

$$\Psi_{K-1}\leq\hat{\psi}_K^{\text{below}}\leq\hat{\psi}_K^{\text{unmodified}}\leq\Psi_K\leq\hat{\psi}_{K+1}^{\text{unmodified}}\leq\hat{\psi}_{K+1}^{\text{above}}\leq\Psi_{K+1}. \tag{B23}$$

Thus, the new $\hat{\psi}_{K+1}$ has to be between $\hat{\psi}_{K+1}^{\text{unmodified}}$ and $\hat{\psi}_{K+1}^{\text{above}}$ such that $\psi_{\odot,K}=\hat{\psi}_K$. In Figure B1b, the levels where the removal of the discontinuities at the interface values has been applied are indicated by black circles.

Acknowledgments

The authors thank P. Bogenschutz and C. Golaz for the helpful discussions. T. Yamaguchi and G. Feingold were supported by the NOAA Climate Program Office through the Climate Process Team and by NOAA's Climate Goal. V. Larson's contributions to this research were supported by the National Science Foundation under grant AGS-0968640. Requests for SAM and CLUBB should be directed to M. Khairoutdinov (marat.khairoutdinov@stonybrook.edu) and V. Larson (vlarson@uwm.edu), respectively. Data used in this paper will be made available by the authors (tak.yamaguchi@noaa.gov) upon request.

References

Ackerman, A. S., et al. (2009), Large-eddy simulations of a drizzling, stratocumulus-topped marine boundary layer, *Mon. Weather Rev.*, *137*(3), 1083–1110, doi:10.1175/2008MWR2582.1.

Arakawa, A. (1975), Modelling clouds and cloud processes for use in climate model, in *The Physical Basis of Climate and Climate Modelling, GARP Publ. Ser.*, vol. 16, pp. 183–197, World Meteorol. Organ., Geneva.

Arakawa, A. (2004), The cumulus parameterization problem: Past, present, and future, *J. Clim.*, *17*(13), 2493–2525, doi:10.1175/1520-0442(2004)017<2493:RATCPP>2.0.CO;2.

Blumofe, R. D., and C. E. Leiserson (1999), Scheduling multithreaded computations by work stealing, *J. ACM*, *46*(5), 720–748, doi:10.1145/324133.324234.

Bogenschutz, P. A., and S. K. Krueger (2013), A simplified PDF parameterization of subgrid-scale clouds and turbulence for cloud-resolving models, *J. Adv. Model. Earth Syst.*, *5*, 195–211, doi:10.1002/jame.20018.

Bogenschutz, P. A., A. Gettelman, H. Morrison, V. E. Larson, D. P. Schanen, N. R. Meyer, and C. Craig (2012), Unified parameterization of the planetary boundary layer and shallow convection with a higher-order turbulence closure in the Community Atmosphere Model: Single-column experiments, *Geosci. Model Dev.*, *5*(6), 1407–1423, doi:10.5194/gmd-5-1407-2012.

Bogenschutz, P. A., A. Gettelman, H. Morrison, V. E. Larson, C. Craig, and D. P. Schanen (2013), Higher-order turbulence closure and its impact on climate simulations in the Community Atmosphere Model, *J. Clim.*, *26*(23), 9655–9676, doi:10.1175/JCLI-D-13-00075.1.

Bony, S., and J.-L. Dufresne (2005), Marine boundary layer clouds at the heart of tropical cloud feedback uncertainties in climate models, *Geophys. Res. Lett.*, *32*, L20806, doi:10.1029/2005GL023851.

Brandt, A. (1977), Multi-level adaptive solutions to boundary-value problems, *Math. Comput.*, *31*(138), 333–390, doi:10.2307/2006422.

Cheng, A., and K.-M. Xu (2006), Simulation of shallow cumuli and their transition to deep convective clouds by cloud-resolving models with different third-order turbulence closures, *Q. J. R. Meteorol. Soc.*, *132*(615), 359–382, doi:10.1256/qj.05.29.

Cheng, A., and K.-M. Xu (2009), A PDF-based microphysics parameterization for simulation of drizzling boundary layer clouds, *J. Atmos. Sci.*, *66*(8), 2317–2334, doi:10.1175/2009JAS2944.1.

Cheng, A., and K.-M. Xu (2013a), Diurnal variability of low clouds in the Southeast Pacific simulated by a multiscale modeling framework model, *J. Geophys. Res. Atmos.*, *118*, 9191–9208, doi:10.1002/jgrd.50683.

Cheng, A., and K.-M. Xu (2013b), Evaluating low-cloud simulation from an upgraded multiscale modeling framework model: Part III: Tropical and subtropical cloud transitions over the northern Pacific, *J. Clim.*, *26*(16), 5761–5781, doi:10.1175/JCLI-D-12-00650.1.

Cheng, A., and K.-M. Xu (2015), Improved low-cloud simulation from the Community Atmosphere Model with an advanced third-order turbulence closure, *J. Clim.*, *28*(14), 5737–5762, doi:10.1175/JCLI-D-14-00776.1.

Cheng, A., K.-M. Xu, and J.-C. Golaz (2004), The liquid water oscillation in modeling boundary layer cumuli with third-order turbulence closure models, *J. Atmos. Sci.*, *61*(13), 1621–1629, doi:10.1175/1520-0469(2004)061<1621:TLWOIM>2.0.CO;2.

Clark, T. L., and R. D. Farley (1984), Severe downslope windstorm calculations in two and three spatial dimensions using anelastic interactive grid nesting: A possible mechanism for gustiness, *J. Atmos. Sci.*, *41*(3), 329–350, doi:10.1175/1520-0469(1984)041<0329:SDWCIT>2.0.CO;2.

Durran, D. R. (1991), The third-order Adams-Bashforth method: An attractive alternative to leapfrog time differencing, *Mon. Weather Rev.*, *119*(3), 702–720, doi:10.1175/1520-0493(1991)119<0702:TTOABM>2.0.CO;2.

Fulton, S. R., P. E. Ciesielski, and W. H. Schubert (1986), Multigrid methods for elliptic problems: A review, *Mon. Weather Rev.*, *114*(5), 943–959, doi:10.1175/1520-0493(1986)114<0943:MMFEPA>2.0.CO;2.

Golaz, J.-C., V. E. Larson, and W. R. Cotton (2002a), A PDF-based model for boundary layer clouds: Part I: Method and model description, *J. Atmos. Sci.*, *59*(24), 3540–3551, doi:10.1175/1520-0469(2002)059<3540:APBMFB>2.0.CO;2.

Golaz, J.-C., V. E. Larson, and W. R. Cotton (2002b), A PDF-based model for boundary layer clouds. Part II: Model results, *J. Atmos. Sci.*, *59*(24), 3552–3571, doi:10.1175/1520-0469(2002)059 < 3552:APBMFB>2.0.CO;2.
Grabowski, W. W. (2001), Coupling cloud processes with the large-scale dynamics using the cloud-resolving convection parameterization (CRCP), *J. Atmos. Sci.*, *58*(9), 978–997, doi:10.1175/1520-0469(2001)058 < 0978:CCPWTL>2.0.CO;2.
Grenier, H., and C. S. Bretherton (2001), A moist PBL parameterization for large-scale models and its application to subtropical cloud-topped marine boundary layers, *Mon. Weather Rev.*, *129*(3), 357–377, doi:10.1175/1520-0493(2001)129 < 0357:AMPPFL>2.0.CO;2.
Griffin, B. M., and V. E. Larson (2016), A new subgrid-scale representation of hydrometeor fields using a multivariate PDF, *Geosci. Model Dev.*, *9*(6), 2031–2053, doi:10.5194/gmd-9-2031-2016.
Guo, H., J. C. Golaz, L. J. Donner, V. E. Larson, D. P. Schanen, and B. M. Griffin (2010), Multi-variate probability density functions with dynamics for cloud droplet activation in large-scale models: Single column tests, *Geosci. Model Dev.*, *3*(2), 475–486, doi:10.5194/gmd-3-475-2010.
Guo, H., J. C. Golaz, and L. J. Donner (2011), Aerosol effects on stratocumulus water paths in a PDF-based parameterization, *Geophys. Res. Lett.*, *38*, L17808, doi:10.1029/2011GL048611.
Guo, H., J.-C. Golaz, L. J. Donner, P. Ginoux, and R. S. Hemler (2014), Multivariate probability density functions with dynamics in the GFDL atmospheric general circulation model: Global tests, *J. Clim.*, *27*(5), 2087–2108, doi:10.1175/JCLI-D-13-00347.1.
Guo, H., J. C. Golaz, L. J. Donner, B. Wyman, M. Zhao, and P. Ginoux (2015), CLUBB as a unified cloud parameterization: Opportunities and challenges, *Geophys. Res. Lett.*, *42*, 4540–4547, doi:10.1002/2015GL063672.
Khairoutdinov, M., and Y. Kogan (2000), A new cloud physics parameterization in a large-eddy simulation model of marine stratocumulus, *Mon. Weather Rev.*, *128*(1), 229–243, doi:10.1175/1520-0493(2000)128 < 0229:ANCPPI>2.0.CO;2.
Khairoutdinov, M., D. Randall, and C. DeMott (2005), Simulations of the atmospheric general circulation using a cloud-resolving model as a superparameterization of physical processes, *J. Atmos. Sci.*, *62*(7), 2136–2154, doi:10.1175/JAS3453.1.
Khairoutdinov, M. F., and D. A. Randall (2001), A cloud resolving model as a cloud parameterization in the NCAR Community Climate System Model: Preliminary results, *Geophys. Res. Lett.*, *28*, 3617–3620, doi:10.1029/2001GL013552.
Khairoutdinov, M. F., and D. A. Randall (2003), Cloud resolving modeling of the ARM summer 1997 IOP: Model formulation, results, uncertainties, and sensitivities, *J. Atmos. Sci.*, *60*(4), 607–625, doi:10.1175/1520-0469(2003)060 < 0607:CRMOTA>2.0.CO;2.
Lappen, C.-L., and D. A. Randall (2001a), Toward a unified parameterization of the boundary layer and moist convection: Part I: A new type of mass-flux model, *J. Atmos. Sci.*, *58*(15), 2021–2036, doi:10.1175/1520-0469(2001)058 < 2021:TAUPOT>2.0.CO;2.
Lappen, C.-L., and D. A. Randall (2001b), Toward a unified parameterization of the boundary layer and moist convection: Part II: Lateral mass exchanges and subplume-scale fluxes, *J. Atmos. Sci.*, *58*(15), 2037–2051, doi:10.1175/1520-0469(2001)058 < 2037:TAUPOT>2.0.CO;2.
Lappen, C.-L., and D. A. Randall (2001c), Toward a unified parameterization of the boundary layer and moist convection: Part III: Simulations of clear and cloudy convection, *J. Atmos. Sci.*, *58*(15), 2052–2072, doi:10.1175/1520-0469(2001)058 < 2052:TAUPOT>2.0.CO;2.
Larson, V. E., and J.-C. Golaz (2005), Using probability density functions to derive consistent closure relationships among higher-order moments, *Mon. Weather Rev.*, *133*(4), 1023–1042, doi:10.1175/MWR2902.1.
Larson, V. E., R. Wood, P. R. Field, J.-C. Golaz, T. H. V. Haar, and W. R. Cotton (2001), Small-scale and mesoscale variability of scalars in cloudy boundary layers: One-dimensional probability density functions, *J. Atmos. Sci.*, *58*(14), 1978–1994, doi:10.1175/1520-0469(2001)058 < 1978:SSAMVO>2.0.CO;2.
Larson, V. E., J.-C. Golaz, and W. R. Cotton (2002), Small-scale and mesoscale variability in cloudy boundary layers: Joint probability density functions, *J. Atmos. Sci.*, *59*(24), 3519–3539, doi:10.1175/1520-0469(2002)059 < 3519:SSAMVI>2.0.CO;2.
Larson, V. E., D. P. Schanen, M. Wang, M. Ovchinnikov, and S. Ghan (2012), PDF parameterization of boundary layer clouds in models with horizontal grid spacings from 2 to 16 km, *Mon. Weather Rev.*, *140*(1), 285–306, doi:10.1175/MWR-D-10-05059.1.
Li, J. L. F., et al. (2012), An observationally based evaluation of cloud ice water in CMIP3 and CMIP5 GCMs and contemporary reanalyses using contemporary satellite data, *J. Geophys. Res.*, *117*, D16105, doi:10.1029/2012JD017640.
Marchand, R., and T. Ackerman (2010), A cloud-resolving model with an adaptive vertical grid for boundary layer clouds, *J. Atmos. Sci.*, *68*(5), 1058–1074, doi:10.1175/2010JAS3638.1.
Miura, H., M. Satoh, T. Nasuno, A. T. Noda, and K. Oouchi (2007), A Madden-Julian oscillation event realistically simulated by a global cloud-resolving model, *Science*, *318*(5857), 1763–1765, doi:10.1126/science.1148443.
Nam, C., S. Bony, J. L. Dufresne, and H. Chepfer (2012), The "too few, too bright" tropical low-cloud problem in CMIP5 models, *Geophys. Res. Lett.*, *39*, L21801, doi:10.1029/2012GL053421.
Randall, D., M. Khairoutdinov, A. Arakawa, and W. Grabowski (2003), Breaking the cloud parameterization deadlock, *Bull. Am. Meteorol. Soc.*, *84*(11), 1547–1564, doi:10.1175/BAMS-84-11-1547.
Seiki, T., C. Kodama, M. Satoh, T. Hashino, Y. Hagihara, and H. Okamoto (2015), Vertical grid spacing necessary for simulating tropical cirrus clouds with a high-resolution atmospheric general circulation model, *Geophys. Res. Lett.*, *42*, 4150–4157, doi:10.1002/2015GL064282.
Sheng, J., and F. Zwiers (1998), An improved scheme for time-dependent boundary conditions in atmospheric general circulation models, *Clim. Dyn.*, *14*(7), 609–613, doi:10.1007/s003820050244.
Sherwood, S. C., S. Bony, and J.-L. Dufresne (2014), Spread in model climate sensitivity traced to atmospheric convective mixing, *Nature*, *505*(7481), 37–42, doi:10.1038/nature12829.
Stevens, B., et al. (2005), Evaluation of large-eddy simulations via observations of nocturnal marine stratocumulus, *Mon. Weather Rev.*, *133*(6), 1443–1462, doi:10.1175/MWR2930.1.
Taylor, K. E. (2001), Summarizing multiple aspects of model performance in a single diagram, *J. Geophys. Res.*, *106*(D7), 7183–7192, doi:10.1029/2000JD900719.
Thayer-Calder, K., et al. (2015), A unified parameterization of clouds and turbulence using CLUBB and subcolumns in the Community Atmosphere Model, *Geosci. Model Dev.*, *8*(12), 3801–3821, doi:10.5194/gmd-8-3801-2015.
Trenberth, K. E., and J. T. Fasullo (2010), Simulation of present-day and twenty-first-century energy budgets of the southern oceans, *J. Clim.*, *23*(2), 440–454, doi:10.1175/2009JCLI3152.1.
Waliser, D. E., et al. (2009), Cloud ice: A climate model challenge with signs and expectations of progress, *J. Geophys. Res.*, *114*, D00A21, doi:10.1029/2008JD010015.
Wang, M., V. E. Larson, S. Ghan, M. Ovchinnikov, D. P. Schanen, H. Xiao, X. Liu, P. Rasch, and Z. Guo (2015), A multiscale modeling framework model (superparameterized CAM5) with a higher-order turbulence closure: Model description and low-cloud simulations, *J. Adv. Model. Earth Syst.*, *7*, 484–509, doi:10.1002/2014MS000375.
Xu, K.-M., and A. Cheng (2013a), Evaluating low-cloud simulation from an upgraded multiscale modeling framework model: Part I: Sensitivity to spatial resolution and climatology, *J. Clim.*, *26*(16), 5717–5740, doi:10.1175/JCLI-D-12-00200.1.
Xu, K.-M., and A. Cheng (2013b), Evaluating low-cloud simulation from an upgraded multiscale modeling framework model: Part II: Seasonal variations over the eastern Pacific, *J. Clim.*, *26*(16), 5741–5760, doi:10.1175/JCLI-D-12-00276.1.

Yang, J., and Q. He (2017), Scheduling parallel computations by work stealing: A survey, *Int. J. Parallel Prog.*, doi:10.1007/s10766-016-0484-8, in press.

Zerroukat, M., N. Wood, and A. Staniforth (2005), A monotonic and positive-definite filter for a semi-Lagrangian inherently conserving and efficient (slice) scheme, *Q. J. R. Meteorol. Soc.*, *131*(611), 2923–2936, doi:10.1256/qj.04.97.

Zhu, P., et al. (2005), Intercomparison and interpretation of single-column model simulations of a nocturnal stratocumulus-topped marine boundary layer, *Mon. Weather Rev.*, *133*(9), 2741–2758, doi:10.1175/MWR2997.1.